



# Optimizing the seeded CVD-growth of uniform graphene films on silicon

Zhichen Yan<sup>1</sup>, Shuangyue Wang<sup>2</sup>, Xianjue Chen<sup>1</sup>, Geedhika K. Poduval<sup>3</sup>, and John A. Stride<sup>1,\*</sup>

<sup>1</sup> School of Chemistry, University of New South Wales, Sydney, NSW 2052, Australia

<sup>2</sup> School of Materials Science and Engineering, University of New South Wales, Sydney, NSW 2052, Australia

<sup>3</sup> School of Photovoltaic and Renewable Energy Engineering, University of New South Wales, Sydney, NSW 2052, Australia

Received: 6 March 2023

Accepted: 23 May 2023

Published online:

5 June 2023

© The Author(s) 2023

## ABSTRACT

Chemical vapor deposition (CVD) has great potential to produce graphene films at large-scale. However, CVD production of graphene films usually requires a catalytic metal substrate, such as copper. Recently we have developed a new method to grow graphene films directly on crystalline silicon wafers with a thermally grown 300 nm oxide layer, using a seeded-CVD growth approach. The use of methane as the feedstock and optimized graphene seeds has led to enhanced film formation, which SEM, X-ray photo-electron and Raman spectroscopies indicate consist of graphene layers formed by the coalescence of expanding “graphene seeds”. The resultant films have regions of single graphene crystallites within them as a result of lateral growth of the seeds. In addition, we have observed that the unilateral conductivity of the graphene films is consistent with the presence of graphene nanoribbons and as such has potential application in device fabrication.

## Introduction

Graphene has the potential to be used as the basis of electronic devices and act the core of the logic circuits as a replacement for silicon [1]. One significant advantage of graphene-based circuitry is the extremely high electron mobility of graphene, allowing graphene-based chips to have much lower power consumption, greater speeds and higher efficiency

than current chips. However, before large-scale application of this remarkable material, there are still many significant barriers which need to be overcome; the most significant one being the lack of appropriate methods to efficiently synthesise graphene in reliable forms.

Chemical vapor deposition (CVD) [2] perhaps has the most potential to facilitate industrial production of large-area graphene films as it has been shown to produce high quality graphene films, however this

Handling Editor: Annela M. Seddon.

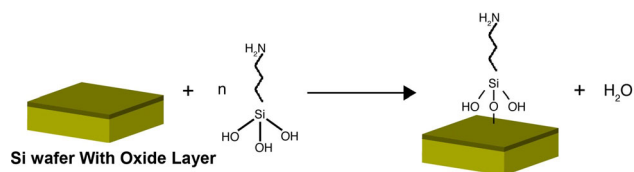
Address correspondence to E-mail: j.stride@unsw.edu.au

usually requires metal substrates (such as copper and nickel) [3]. This is due to the high adsorption capacity of certain metals to carbon that results in the metallic substrate acting as a catalyst, leading to graphene growth. However, the requirement to subsequently transfer the films to insulating or semi-conducting substrates (such as silicon or silicon dioxide), can lead to further problems such as contamination and the introduction of defects, significantly impacting the properties (such as carrier mobility) of the films [4]. This has led to increased focus on metal-free CVD production of graphene [5]. Thus far this has seen limited success, partly due to the lower carbon affinity of substrates such as silicon (or other non-metals) compared to many metallic elements. In the absence of nucleation sites, the surface concentrations of the carbon species (usually methane or ethanol) need to be extremely high in order to induce carbon atom deposition on the surface of silicon and subsequent film formation. However, at the high surface concentrations of carbon species required in order to nucleate carbon on silicon, secondary nucleation processes occur at the sites of initial graphene-like monolayers [6]. As a result, post-CVD processed films often contain additional graphene layers or become bowl-shaped [6]. An alternative approach has been reported to use a copper layer above a sacrificial carbon source in the CVD growth of relatively high quality graphene films [7], which of course is not strictly metal-free.

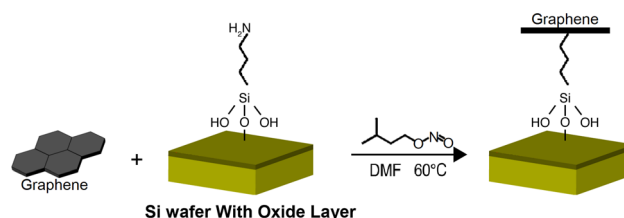
The Tour reaction [8] is well-known and is widely used to modify carbon nanotubes and graphene; it makes use of an aryl diazonium intermediate (formed by aniline derivatives and isoamyl nitrite) to add phenyl groups to carbon surfaces via radical reactions. Another widely-used reaction in surface chemistry is that of 3-trimethoxysilyl-1-propanamine (APS) [9] which is routinely used to fix DNA onto glass or silicon dioxide by the tethering of amine ( $-NH_2$ ) units to the substrate surface, Scheme 1

By combining these two reactions, small graphene flakes (produced by the Hummer's method [10]) can act as “graphene seeds” on silicon wafers with an oxide layer, Scheme 2, even in the absence of aryl groups.

In this paper, fixed “graphene seeds” were used as the primary nucleation sites to grow graphene films in a CVD process. In order to ensure that the carbon atoms are deposited only at the edge of the seeds to result in uniform graphene films, key factors such as



**Scheme 1** Reaction of APS attaching to silicon dioxide.



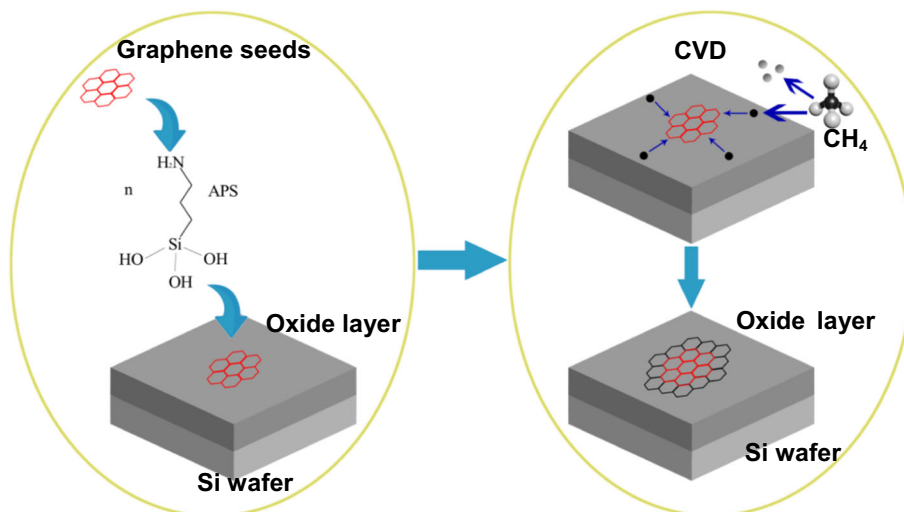
**Scheme 2** “Graphene seed” fixed process via APS on monocrystalline silicon.

the flow-rate of various carbon sources must be precisely controlled, Fig. 1. We have found that the ratio of methane to hydrogen in the feedstock flow is highly significant in the CVD-growth of graphene films. At relatively low concentrations of carbon, a carbon-bearing species must be adsorbed near to the edge of an existing graphene flake for a sufficient time to react. In real experiments, a hydrogen partial pressure is used to generate a reductive atmosphere and carbon diluent; as such, it is an important parameter impacting the production of graphene films. Whilst the precise role that hydrogen plays in CVD remains unclear, it is generally assumed that it modifies both the surface concentration of carbon-bearing species and the configuration at the edge of graphene sheets by hydrogenation and dehydrogenation reactions; these factors then determine the dynamics of surface species to attach at the graphene edges [11]. In this paper, we used equivalent 30 sccm methane and hydrogen as the CVD feedstock, based on a balance between the quality and efficiency of produced graphene.

## Experimental

All chemicals were obtained from Sigma-Aldrich and used without further purification. Deionized (DI) water was used throughout the syntheses.

**Figure 1** Schematic representation of metal-free CVD experimental set-up of graphene production.



### Graphene oxide

The “graphene seed” (graphene oxide) used in this work was produced by a modified Hummer’s method and was obtained in powder form. 2 g graphite powder (0.166 mol) and 4 g potassium permanganate (0.050 mol) was added to 46 mL of 96% concentrated sulfuric acid (0.86 mol). The reaction temperature was maintained below 4 °C whilst stirring for 2 h in order to mix the reactants homogeneously. For the graphite oxidation stage, the reaction temperature was raised to 40 °C for a further 30 min of stirring and then increased to 95 °C with addition of 50 mL DI water. Under these conditions, aqueous species intercalate between the graphitic layers, sharply increasing the inter-planar separation to yield few- and single-layer graphene oxide. The final product washed by centrifugation (4–5 times in DI water) until the supernatant liquid was transparent; the supernatant liquid was then removed and the sediment placed in a vacuum oven to dry for 12–24 h.

### Graphene seeds

In order to obtain high quality graphene seeds, the Hummer’s derived graphene powders were first treated ultrasonically: 5 mg of the dry powdered graphene oxide was dispersed in 20 mL of dimethyl formamide (DMF, 0.26 mol) and a Carbon Ultrasonic Apparatus probe (20% energy for 1 h) was used to homogeneously mix the solution; this was then centrifuged (6000 rpm for 1 h) and the top 5 mL of the solution extracted for further processing.

### Seed tethering

To prepare the Si wafer prior to the pseudo-Tour reaction, a 300 nm SiO<sub>2</sub> layer was thermally deposited in order to enable reaction with APS. The surface of the Si/SiO<sub>2</sub> wafer was first cleaned in an ultrasonic bath for 15 min using DI water and ethanol and then dried in a vacuum oven. The cleaned wafer was then bathed in a pre-mixed 4% solution of APS (4 mL, 0.022 mol) in acetone (100 mL, 1.36 mol) for 4 min at room temperature. The wafer, now with APS attachments, was placed into a glass reaction vessel and 10 mL of the centrifuged graphene solution added. Isoamyl nitrite (4.4 mL, 0.032 mol) in DMF (40 mL, 0.52 mol) was then added in one step and continuously stirred for 12 h at 80 °C. Finally, the modified silicon wafer was cleaned for 5 min in an ultrasonic bath with ethanol and then DI water for a further 5 min; it was then dried in a vacuum oven. In the meantime, as a control experiment, Si wafers both with and without APS, were prepared and treated identically with respect to the Tour reaction.

### CVD growth

The Si wafer with graphene seeds tethered by APS was placed into the CVD reaction chamber with the seeded face exposed. A methane carbon source (30 sccm CH<sub>4</sub> and 30 sccm H<sub>2</sub>) was passed over the substrate which was held at 950 °C (increasing from room temperature at 30 °C/min) for a given CVD reaction time. After CVD growth, an extra annealing process was used in order to release residual stresses in the film. Initially the temperature of the reaction

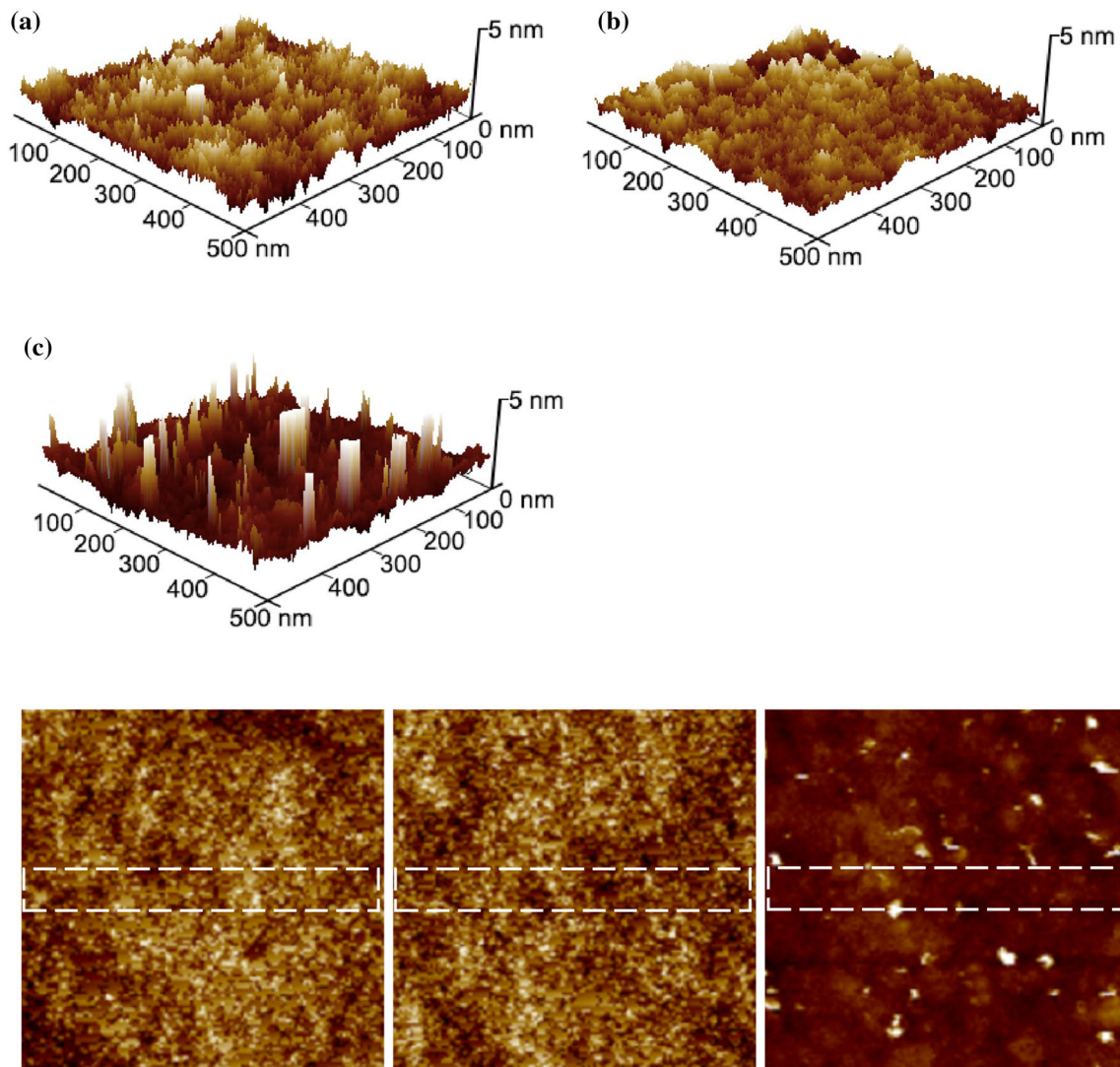


**Figure 2** AFM images of the surface of the **a** raw Si wafer complete with the 300 nm SiO<sub>2</sub> layer; **b** the same raw Si wafer; **c** another Si wafer with “graphene seed” both post treatment of

chamber was held at 950 °C for 0.5 h and was then cooled to an intermediate temperature (475 °C) at a rate of 10 °C/min and held for 0.5 h, under protective gas (30 sccm H<sub>2</sub>).

### Characterisation

Atomic force microscopy (AFM) was performed using a Bruker ICON SPM in contact mode with a 512 point scan line. Scanning electron microscopy (SEM) images were obtained on a FEI Co. NanoSEM 450, under a 5 kV accelerating voltage. Raman spectra were measured on a Renishaw inVia spectrometer, using 532 nm laser excitation. Surface conductivity

4.0 h CVD processing (methane as the carbon source) and **d** two-dimensional view and roughness analysis [within the dotted line] of (a), (b) and (c) [from left to right].

was detected using an Environmental Scanning Probe Microscope (JSPM 5400, produced by Nihon Denshi [JEOL]).

### Results and discussion

#### Film growth

Comparing the AFM images of the raw Si wafer with a 300 nm surface oxide layer (Fig. 2a) and the same wafer after 4.0 h of CVD with 30 sccm CH<sub>4</sub> and 30 sccm H<sub>2</sub> (Fig. 2b), it is clear that the surface of the unseeded Si wafer before and after CVD processing was



**Figure 3** SEM results of the raw Si wafer complete with the 300 nm SiO<sub>2</sub> layer before and after CVD processing **a** on a Si wafer without APS and the Tour-like reaction with raw graphene; **b** on a Si wafer with APS-tethered raw graphene flakes; **c** on a Si wafer with APS-tethered centrifuged graphene flakes.

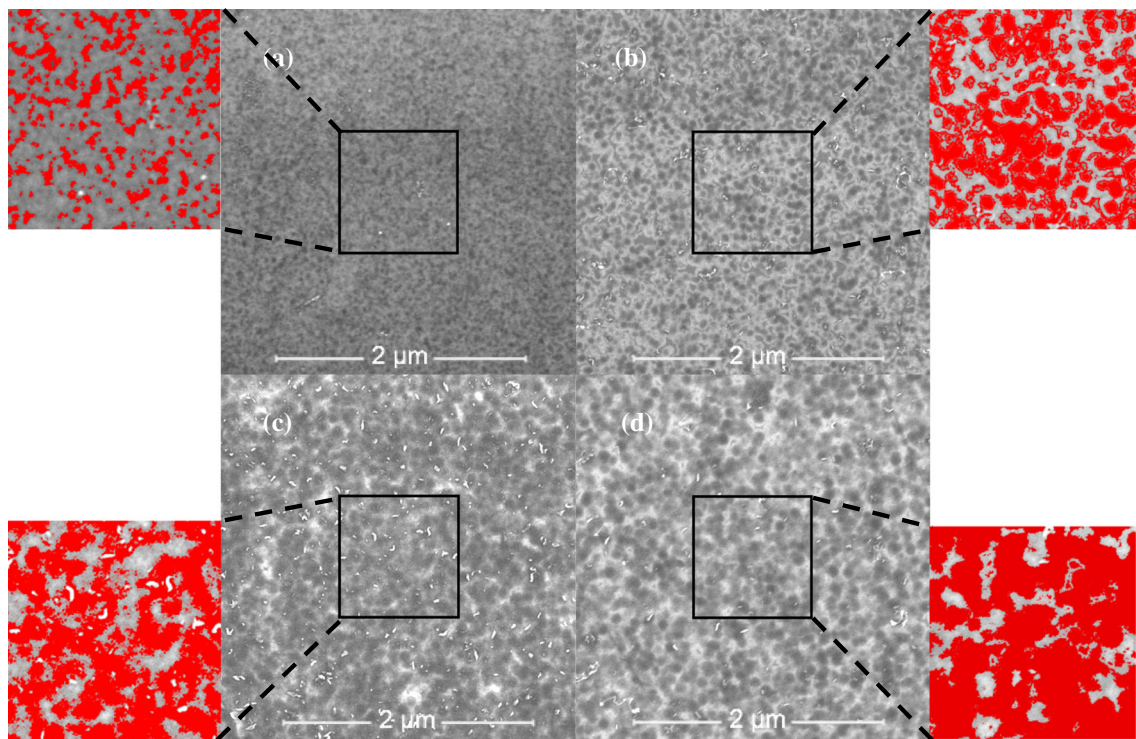
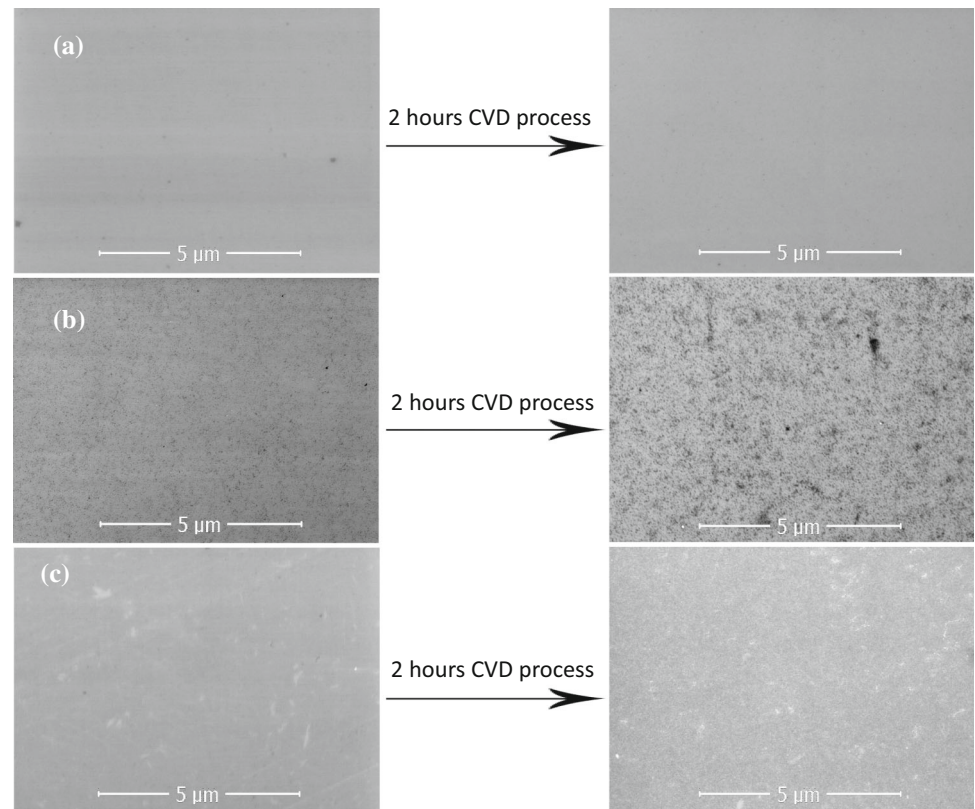


**Figure 4** SEM results of the raw Si wafer complete with the 300 nm SiO<sub>2</sub> layer and post treatment with APS-tethered centrifuged graphene flakes, and then after **a** 2.0 h CVD; **b** 4.0 h CVD; **c** 7.0 h CVD; **d** 9.0 h CVD.

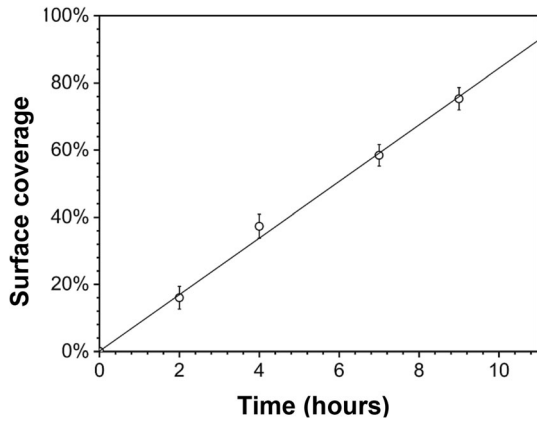


**Figure 5** Linear growth profile of the Si wafer (complete with the 300 nm SiO<sub>2</sub> layer and post treatment with APS-tethered centrifuged graphene flakes) expressed as percentage of coverage of graphene at different CVD growth times.  $R^2 = 0.999$ , Growth Rate =  $8.428 \pm 0.188\%/h$ .

near atomically-flat; according to the roughness analysis of AFM, the average roughness ( $R_a$ , the arithmetic average of the deviations from the centre plane across a region of the surface) was only 0.208 and 0.218 nm, respectively, for the un-seeded Si wafer before and after 4 h the CVD process, whilst the root mean square roughness ( $R_q$ , the standard deviation of the vertical values within a given area of the surface) values were 0.261 and 0.272 nm. Meanwhile the graphene-seeded wafer treated to the same CVD processing (Fig. 2c) clearly shows changes to the surface morphology, with  $R_a = 0.878$  and  $R_q = 1.43$  nm. This indicates that the graphene seeds are

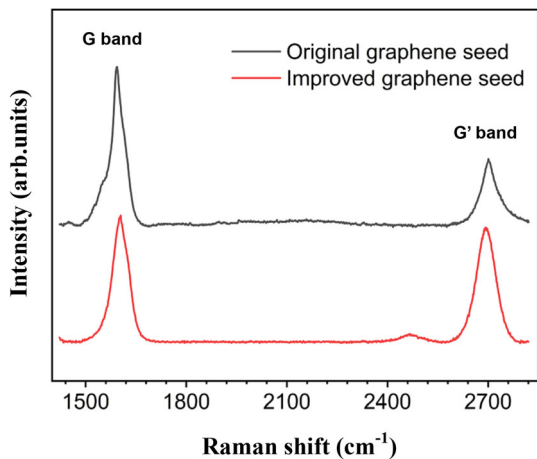


**Figure 6** Raman spectra obtained at 532 nm laser excitation: decorated Si with original and improved “graphene seed” after 2.0 h CVD process.

necessary to achieve film growth under the reaction parameters used.

Figure 3 shows SEM images of Si wafers under a range of treatment conditions; the CVD reaction conditions used in this series of experiments was a continuous methane/hydrogen flow (30 sccm CH<sub>4</sub> and 30 sccm H<sub>2</sub>) at 950 °C for 2 h. Figure 3a has images of a Si wafer without APS attached both before and after the Tour-like reaction with non-centrifuged graphene from the Hummer’s method. In contrast, Fig. 3b has images of a Si wafer with APS attached both before and after the reaction with non-centrifuged graphene from the Hummer’s method. Finally Fig. 3c has images of a Si wafer with APS attached both before and after reaction with centrifuged graphene.

After 2 h of CVD processing, Si substrates having tethered graphene seeds clearly show growth about the graphene islands on the surface (although very small under SEM), that is absent from the neat Si substrate (Fig. 3a post CVD). SEM images of the Si wafer with APS-tethered raw graphene (Fig. 3b) has obvious signs of graphene/graphitic dot-like species even before the CVD processing. After 2 h of CVD processing the density of these carbon dots is similar to the Si wafer treated with centrifuged graphene (Fig. 3c), but the growth appears to be less uniform and in some regions, appear to have graphitized.

The conclusion that we draw from these results is that blank Si wafers that are not patterned with graphene seeds undergo no graphene growth under CVD. This finding supports the notion that in CVD,

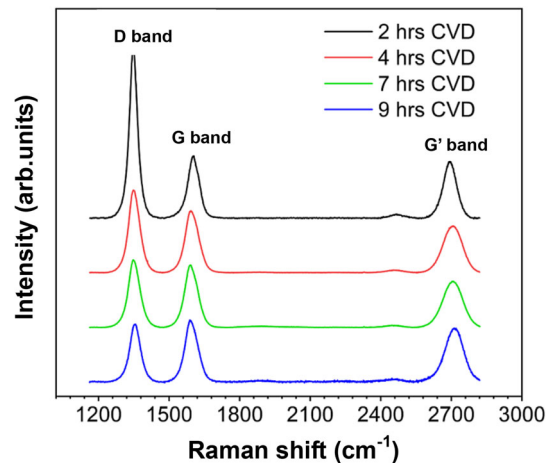


**Figure 7** Raman spectroscopy results by 532 nm laser: decorated Si with “graphene seed” (which was treated by centrifugation process) after 2.0–9.0 h CVD process.

carbon atoms are only deposited at the edge of the seed particles and not elsewhere. Secondly, by comparing the results of Si wafers with APS-tethered raw (Fig. 3b) and centrifuged graphene (Fig. 3c), then the quality of the “graphene seed” has a direct impact on the final film. Thirdly, centrifuging the graphene effectively eliminates graphene flakes that have many layers, effectively nano-graphite particles, leading to the growth of higher quality graphene films under CVD.

Figure 4 shows the SEM images of Si wafers treated with the improved, centrifuged graphene seeds, fixed with APS and reacted under CVD for between 2.0 and 9.0 h. It is clear that the size of the graphene islands increase with increasing reaction time, and after 9.0 h of CVD, more than 75% of the total surface area was covered by the grown films.

By analyzing the ratio of pixels of different bright areas of the SEM images, a percentage coverage of the graphene film can be obtained. Comparing this value at different CVD reaction times, we obtained the temporal growth profile of the films, which approximates to a linear growth up to 9.0 h of CVD reaction time (Fig. 5). It can be seen that after 9.0 h CVD processing, the percentage coverage of grown graphene film reached more than 75% (the initial value was below 0.01%, Fig. 3c, left). After 11 h, nearly 90% coverage should be projected based on this growth profile; however at times beyond 9 h CVD time, growth of individual graphene islands increasingly led to the overlap of sheets and associated rapid changes in shape, including curling, as continued deposition resulted in more graphite-like films.

### Raman spectroscopy

Graphene has three main bands in the Raman spectrum, labeled as the **G**, **D** and **G'** bands [12]. The **G** band is due to in-plane vibrations of the  $sp^2$  carbon atoms and is the major characteristic feature of many allotropes of carbon. The position of the **G** band in graphene is around  $1585\text{ cm}^{-1}$  and the intensity can be expected to rise approximately linearly along with

**Table 1** The  $(I_D/I_G)^{-1}$  of produced graphene film after different CVD reaction times

	2 h CVD	4 h CVD	7 h CVD	9 h CVD
$(I_D/I_G)^{-1}$	0.381	0.750	0.922	1.063

**Table 2** Relative values of  $S$  of produced graphene film calculated by the percentage of coverage of graphene film

	$\theta S_2$	$\theta S_4$	$\theta S_7$	$\theta S_9$
	0.160	0.373	0.584	0.753

**Table 3** The relative increase of  $L^2$  and  $\theta S$  of the graphene film at different growth times (relative to 2.0 h of CVD)

	Relative increase		
	2.0–4.0 h	2.0–7.0 h	2.0–9.0 h
$L^2$	196.9%	242.0%	279.0%
$\theta S$	233.1%	365.0%	470.6%

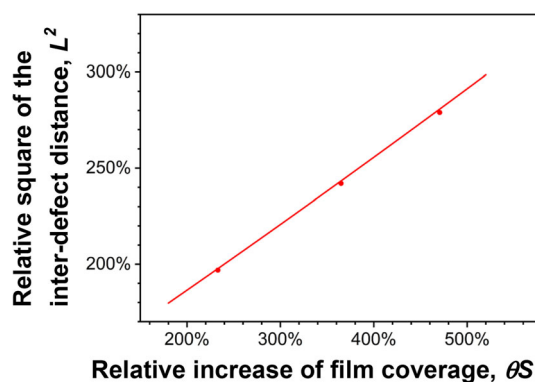


**Figure 8** Plot of reduced values of  $L^2$  against  $S$  (relative to 2.0 h of CVD growth),  $R^2 = 0.99836$ .

the increase of number of layers of graphene, in line with there being more carbon atoms bonded in multilayer graphene. The **G'** band is usually at about  $2700\text{ cm}^{-1}$  and can be used to indicate the degree of interlayer stacking; it is also the main characteristic peak of graphene. The **G'** band is related to the energy band structure of graphene and is due to a second-order two phonon resonance. For single-layer graphene, the intensity of the **G'** band ( $I_{G'}$ ) is higher than the **G** band ( $I_G$ ); however,  $I_{G'}$  decreases significantly when the number of layers increases, coupled to a blue shift in frequency [11].

Figure 6 shows the Raman spectra of Si decorated with raw and centrifuged graphene seeds after just 2.0 h of CVD processing, excited by a 532 nm laser. By comparing the results with standard Raman spectroscopy of graphene [13] and the SEM results of different samples after 2.0 h CVD process (Fig. 3), it can be seen that after CVD, the  $I_{G'}/I_G$  of the centrifuged graphene seeds is much higher than that



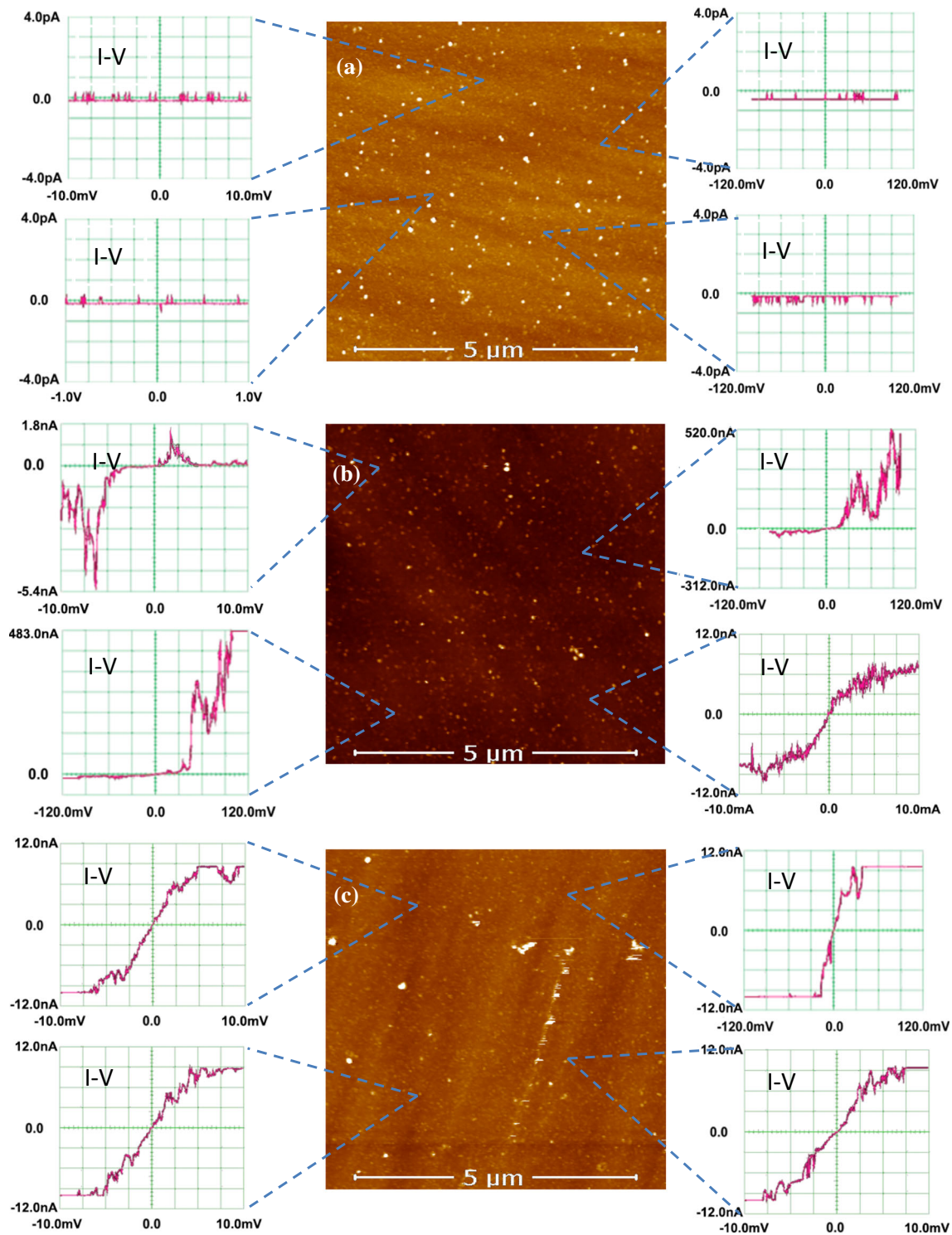


**Figure 9** The surface conductivity results of decorated Si wafer with “graphene seed” (which was treated by centrifugation process), **a** before CVD process; **b** after 2.0 h CVD process; and **c** after 4.0 h CVD process; with methane as carbon source.

from the raw-seeds, indicating that the graphene film produced from the centrifuged seeds consists of fewer layers, estimated to average 2, as opposed to more “graphitization level” for the less refined seeds.

Graphene containing defects, which can occur within the sheet or at edge sites, has another main band in the Raman spectrum called the **D** band [14][15]. Whilst its position, at  $1350\text{ cm}^{-1}$ , is almost



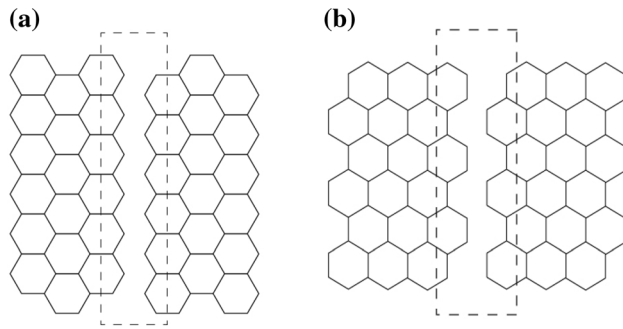


**Figure 10** a Zig-zag and b armchair graphene nanoribbons.

half that of the  $G'$  band the  $G'$  band is not the frequency-doubling signal of  $D$ ; the  $D$  band results from a double resonance Raman process related to defect scattering. The intensity ratio of the  $D$  and  $G$  bands ( $I_D/I_G$ ) [13] can be used to indicate the defect density or edge sites of a graphene sheet. Figure 7 is the Raman spectrum of Si decorated with centrifuged graphene seeds after 2.0–9.0 h of CVD processing and excited by a 532 nm laser which shows how the  $G'$  grows, but so too the relative strength of  $D$ .

Assuming that all of the defects in a graphene sheet are zero-dimensional point defects, and defining the average distance between two defects to be  $L$  with the laser energy used  $E_L$ , Ferrari et al. reported that  $L$  can be related to  $I_D/I_G$  and  $E_L$  [16]:

$$L^2(\text{nm}^2) = \frac{(4.3 \pm 1.3) \times 10^3}{E_L^4 \times \left(\frac{I_D}{I_G}\right)} \quad (1)$$

Given that all Raman spectra obtained here were measured at the same wavelength (532 nm), the terms  $(4.3 \pm 1.3) \times 10^3$  and  $E_L^4$  are constant, yielding  $L^2 \propto (I_D/I_G)^{-1}$ . Taking values of the  $(I_D/I_G)^{-1}$  after 2.0, 4.0, 7.0 and 9.0 h of CVD growth, we can extract growth information (Table 1):

Meanwhile, the SEM images, Fig. 4, also provide a representation of relative growth at different CVD times, assuming that the initial density of graphene seeds is constant. With a given number of graphene seeds (equal to  $n$ ) within an imaged area,  $f$ , and the percentage area of graphene film coverage as  $C$ , then the average size of grown graphene sheets ( $S$ ) in the test area is  $S = C \cdot f/n$ . If one uses a common area,  $f$ , then the  $f/n$  is constant and  $S \propto C$ , in which case  $C$  can be obtained from the SEM images (Fig. 4). The relative growth ( $\theta S$ ) after 2.0, 4.0, 7.0 and 9.0 h of CVD processing can be calculated, Table 2.

Taking ratios of the data held in Tables 1 and 2 to that at 2.0 h, the relative increased growth of  $L^2$  and  $S$  at different growth times can be calculated, Table 3.

$$R_{\theta S} = \theta S_2 / \theta S_{2+\Delta t} \quad R_L^2 = L_2^2 / L_{2+\Delta t}^2 \quad (2)$$

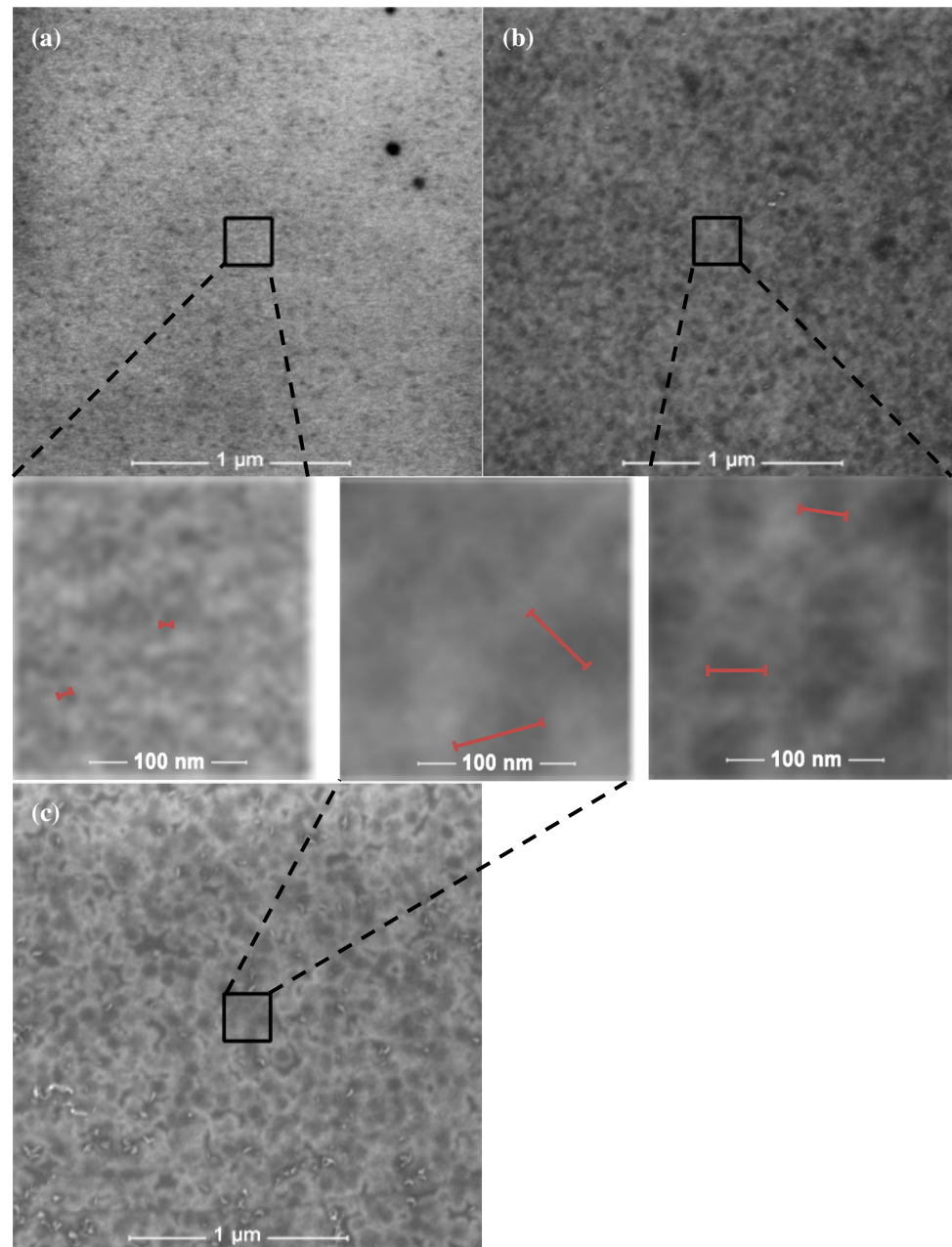
A plot of  $\theta S$  against  $L^2$  will be linear if both values are accurate representations of graphene film growth, Fig. 8 ( $R^2 = 0.99836$ ). The strong linear correlation between the relative increase in  $L^2$  and  $\theta S$ , means that the main defect sites in the growing graphene islands are at the edges as the distance between defects is proportional to the average diameter of the graphene sheets. Meanwhile, the coverage  $S$  is proportional to the square of the average diameter. The density of other defect sites can therefore be considered to be low and that as such, the quality of the grown film is high.

In addition, the Raman spectroscopy results (Fig. 7) also show that with the increase in CVD reaction time,  $I_{G'}/I_G$  basically remains unchanged, indicating that even after relatively long CVD reaction times, the number of layers of graphene sheets remains invariant, providing additional evidence that the produced graphene films approximately maintain the original laminar structure of the seeds and grow uniformly in 2-dimensions only.

## Electrical properties

The surface conductivity of Si decorated with centrifuged graphene seeds before and after 2.0 or 4.0 h of CVD  $\text{CH}_4/\text{H}_2$  processing was studied using a JSPM 5400, Fig. 9. Due to the fact that the graphene seeds are very small and not continuous, the surface of the Si wafer with seeds attached was found to be barely conductive and similar to that of raw silicon with a  $\text{SiO}_2$  layer (Fig. 9a). For the same Si wafer after 2.0 h CVD (Fig. 9b), some areas were found to show unilateral conductivity, a unique electrical property of PN junctions; this phenomenon is probably due to some graphene seeds growing to an appropriate size (width  $< 50$  nm) with an armchair chirality. With sufficient reaction time they turn into GNRs (Fig. 10) that display semiconductor properties, i.e. undergo a band gap opening; however, defect sites can also result in gapped states. In the meantime, impurities or defects may combine with the GNRs to form  $p$ -type or  $n$ -type GNRs, eventually forming PN-junctions with the substrate. At the increased CVD time of 4.0 h (Fig. 9c), the unilateral conductivity

**Figure 11** SEM results of **a** the surface of the raw Si wafer complete with the 300 nm SiO<sub>2</sub> layer and post treatment with APS-tethered centrifuged graphene flakes; **b** same Si wafer after 2.0 h CVD process; **c** same Si wafer after 4.0 h CVD process with methane as carbon source (red line indicate the width of graphene flakes).



disappeared with the graphene film showing typical metallic behaviour, possibly due to the GNRs growing or coalescing as their width increases. These experiments verified that the band gap decreases with an increase of GNR width [17], eventually reaching zero, rendering the grown graphene films to be electronic conductors.

### Nano-structure of films

Graphene nano-ribbons (GNRs) are a specific form of graphene, having a width of less than 50 nm and an

aspect ratio greater than 2. There are two kinds of GNR—“zig-zag” (Fig. 10a) and “armchair” (Fig. 10b)—basically dependent on the edge structures of the ribbon. GNRs can show different electrical properties based on the different chiralities. According to tight-binding calculations [18], zig-zag GNRs are metallic, whilst armchair GNRs can be either semiconducting or metallic, depending upon the width.

Several methods have been used to produce GNRs, such as “axially cutting nanotubes [19]” and “bottom-

up synthesis [20]”, etc., but none of these current methods actually meet production requirements. The approach used in this work to produce graphene films may provide a new way to obtain GNRs if greater control over the growth processes can be achieved. Figure 11a is the SEM image of a Si wafer with a 300 nm SiO<sub>2</sub> layer, post treatment with APS-tethered centrifuged graphene flakes. It can be seen that before CVD processing, the average size of the graphene seed is very small, with diameters of only a few nanometers. As most of the fixed “graphene seeds” are very small (~ nm), they are barely detected prior to CVD treatment, however some have been shown to grow to significant sizes (about 50 nm, Fig. 11b) in order to be considered as GNRs after 2.0 h of CVD growth with 30 sccm CH<sub>4</sub> and 30 sccm H<sub>2</sub>. After 4.0 h of CVD growth, the size further increased to more than 70 nm (Fig. 11c). On the other hand, Si decorated with “graphene seeds” post 2.0 h of CVD processing, still have areas that show I–V curves of both linearly varying and atypical unidirectional conductivity (Fig. 9b), indicating that the final products are not uniform and that the whole area does not show a single electronic structure or behave as a single PN junction. Whilst this new method of producing graphene films may potentially be used to open the band gap of graphene-related materials, it will require further research and improvements before it can be used in practical applications.

## Conclusion

Growth of graphene films directly on silicon using CVD is very attractive for a range of applications and has the potential to avoid introducing defects. Using a seeded-CVD growth, we have shown that the quality of the graphene flake seeds was significantly improved by using a simple purification method, which results in high quality graphene films after CVD processing. Electrical measurements demonstrate that regions of the films behave as GNRs, with an opening of the graphene band-gap. These initial results lead to the potential for practicable design of logic structures such as PN and PNP junctions within highly uniform graphene films incorporating GNRs.

## Acknowledgements

We would thank staff and facilities in Schools of Chemistry, Materials Science and Engineering, Photovoltaic and Renewable Energy Engineering, and Mark Wainwright Analytical Centre and Spectroscopy Laboratory for the support and assistance during the experimental phase at the University of New South Wales.

## Funding

Open Access funding enabled and organized by CAUL and its Member Institutions.

## Declarations

**Conflict of interest** The authors declare that they have no conflict of interest.

**Open Access** This article is licensed under a Creative Commons Attribution 4.0 International License, which permits use, sharing, adaptation, distribution and reproduction in any medium or format, as long as you give appropriate credit to the original author(s) and the source, provide a link to the Creative Commons licence, and indicate if changes were made. The images or other third party material in this article are included in the article's Creative Commons licence, unless indicated otherwise in a credit line to the material. If material is not included in the article's Creative Commons licence and your intended use is not permitted by statutory regulation or exceeds the permitted use, you will need to obtain permission directly from the copyright holder. To view a copy of this licence, visit <http://creativecommons.org/licenses/by/4.0/>.

## References

- [1] Novoselov K (2004) Electric field effect in atomically thin carbon films. *Science* 306(5696):666–669
- [2] Wang M et al (2016) CVD polymers for devices and device fabrication. *Adv Mater* 29(11):1604606
- [3] Kalita G, Tanemura M (2017) Fundamentals of chemical vapor deposited graphene and emerging applications. In: Kyzas GZ, Mitropoulos AC (eds) *Graphene materials advanced applications*. InTech



- [4] Kim J, Woo J, Jo S, Oh J, Hong W, Lee B, Jung H, Kim J, Roh S, Han C (2020) Clean and less defective transfer of monolayer graphene by floatation in hot water. *Appl Surf Sci* 508:145057
- [5] Yan Z, Joshi R, You Y, Poduval G, Stride J (2021) Seeded growth of ultrathin carbon films directly onto silicon substrates. *ACS Omega* <https://doi.org/10.1021/acsomega.0c05770>
- [6] Tai L, Zhu D, Liu X, Yang T, Wang L, Wang R, Jiang S, Chen Z, Xu Z, Li X (2017) Direct growth of graphene on silicon by metal-free chemical vapor deposition. *Nano-Micro Lett* 10(2):20
- [7] Zhuo Q, Mao Y, Lu S, Cui B, Yu L, Tang J, Sun J, Yan C (2019) Seed-assisted synthesis of graphene films on insulating substrate. *Materials* 12(9):1376
- [8] Price B, Tour J (2006) Functionalization of single-walled carbon nanotubes “on water.” *J Am Chem Soc* 128(39):12899–12904
- [9] Vrancken K, Casteleyn E, Possemiers K, Van Der Voort P, Vansant E (1993) Modelling of the reaction-phase interaction of  $\gamma$ -aminopropyltriethoxysilane with silica. *J Chem Soc Faraday Trans* 89(12):2037–2040
- [10] Chong S, Lai C, Abd Hamid S, Low F, Liu W (2015) Simple preparation of exfoliated graphene oxide sheets via simplified Hummer’s method. *Adv Mater Res* 1109:390–394
- [11] Li P, Li Z, Yang J (2017) Dominant kinetic pathways of graphene growth in chemical vapor deposition: the role of hydrogen. *J Phys Chem C* 121(46):25949–25955
- [12] Malard L, Pimenta M, Dresselhaus G, Dresselhaus M (2009) Raman spectroscopy in graphene. *Phys Rep* 473(5–6):51–87
- [13] Ni Z, Wang Y, Yu T, Shen Z (2008) Raman spectroscopy and imaging of graphene. *Nano Res* 1(4):273–291
- [14] Eckmann A, Felten A, Mishchenko A, Britnell L, Krupke R, Novoselov K, Casiraghi C (2012) Probing the nature of defects in graphene by Raman spectroscopy. *Nano Lett* 12(8):3925–3930
- [15] Hulman M (2014) Raman spectroscopy of graphene. *Graphene*. Elsevier, pp 156–183
- [16] Cañado L, Jorio A, Ferreira E, Stavale F, Achete C, Capaz R, Moutinho M, Lombardo A, Kulmala T, Ferrari A (2011) Quantifying defects in graphene via Raman spectroscopy at different excitation energies. *Nano Lett* 11(8):3190–3196
- [17] Han M, Özyilmaz B, Zhang Y, Kim P (2007) Energy band-gap engineering of graphene nanoribbons. *Phys Rev Lett* 98(20):206805
- [18] Guan J, Xu L (2021) Energy gaps in BN/gnrs planar heterostructure. *Materials* 14(17):5079
- [19] Kosynkin D, Higginbotham A, Sinitskii A, Lomeda J, Dimiev A, Price B, Tour J (2009) Longitudinal unzipping of carbon nanotubes to form graphene nanoribbons. *Nature* 458(7240):872–876
- [20] Narita A, Feng X, Müllen K (2014) Bottom-Up synthesis of chemically precise graphene nanoribbons. *Chem Rec* 15(1):295–309

**Publisher’s Note** Springer Nature remains neutral with regard to jurisdictional claims in published maps and institutional affiliations.